Landslides (2014) 11:711–722
DOI 10.1007/s10346-013-0447-8
Received: 18 June 2013
Accepted: 29 October 2013
Published online: 14 November 2013

Xueliang Wang · Paolo Frattini · G. B. Crosta · Luqing Zhang · Federico Agliardi · Serena Lari · Zhifa Yang

Uncertainty assessment in quantitative rockfall risk assessment

Abstract This study shows a quantitative rockfall risk assessment (QRA) for a slope of the Feifeng Mountain (China), including an explicit assessment of the uncertainties. For rockfall risk analysis, the annual probability of occurrence, reach probability, temporal–spatial probability and vulnerability of tourists were calculated for both dry and rainy day conditions. The resulting individual risk for exposed people visiting the historical site can be considered as acceptable for all scenarios, whereas the overall societal risk lies within the as low as reasonably practicable (ALARP) zone and therefore requires some mitigation actions. For the explicit assessment of uncertainty, an error propagation technique (first-order second moment (FOSM)) was adopted, starting from expert knowledge heuristic estimations of the coefficient of variation for each component of the risk analysis procedure. As a result, coefficients of variation of the calculated risk were obtained, ranging from 48 to 132%, thus demonstrating the importance of accounting for uncertainty in rockfall risk modelling. A multi-criteria methodology is also proposed for the assessment of the standard deviation of the parameters adopted for the stochastic rockfall run-out model.

Keywords Rockfall · Quantitative risk assessment · Uncertainty · FOSM · 2D rockfall modelling · Individual risk · Societal risk

Introduction

Rockfall risk analysis is inherently complex and difficult. Such difficulties derive from several factors: lack of accurate data, strongly site-specific nature of rockfall, difficulty in quantifying and modelling spatial rockfall distribution, quantifying the heterogeneity of vulnerability of different elements at risk and variability in temporal vulnerability (Glade 2003; Crosta and Agliardi 2004; Michoud et al. 2012; Frattini et al. 2008, 2012).

Rockfall risk can be defined as a measure of probability and severity of an adverse effect to health, property or the environment (Hungr et al. 1999; Zhang et al. 2004; Corominas et al. 2005; Fell et al. 2008). Rockfall risk for exposed people can be estimated by the product of three conditional probabilities (annual probability of occurrence, reach probability and temporal–spatial probability) and vulnerability, summed up for all the considered scenarios.

The annual probability of occurrence of a rockfall event, $P(L)$, is modelled in the literature by using historical data in order to assess a frequency of events which can be converted into an exceedance probability by using an appropriate probabilistic model (e.g. Poisson or binomial). Since the frequency is recognised to depend on rockfall volume, frequency–magnitude relationships have been used in the literature (Hungr et al. 1999; Guzzetti et al. 2002a). $P(L)$ may also be determined by establishing relationships with triggering event frequencies (e.g. rainfall, earthquake) with known annual exceedance probabilities. However, because of the different site-specific characteristics, the lack of statistically sound historical inventories and the difficulty to model slope stability along the cliffs, the assessment of probability of occurrence is affected by large uncertainties. Moreover, the conditions responsible for a given landslide frequency in the past may no longer exist, due to climatic or land use changes (Cascini et al. 2005).

The reach probability, $P(T|L)$, depends on the propagation of rockfalls along the slope, and it is controlled by slope surface morphology (e.g. slope gradient, curvature), slope roughness, block material, slope deposit grain size and vegetation (Azzoni et al. 1995; Jones et al. 2000; Crosta and Agliardi 2004). Several approaches have been used to assess rockfall run-out, such as empirical methods (shadow angle or reach angle methods) (Evans and Hungr 1993; Corominas 1996) or mathematical modelling in 2D (Stevens 1998; Jones et al. 2000) or 3D (Guzzetti et al. 2002b; Crosta et al. 2004; Dorren et al. 2006). Empirical approaches are useful for a preliminary estimation of rockfall susceptibility, but they are unsuitable for risk analysis because they do not provide the frequency of blocks passing through each position along the slope, without the introduction of strong simplifications (Copons et al. 2009). Hence, mathematical models are needed for risk analysis. However, large uncertainties exist in computing the trajectory and the arrest of blocks along the slope. These uncertainties are related to the size, shape and mechanical properties of the rockfall blocks; the relevant parameters in the modelling and their variation in space and time, but also the geometrical and mechanical characteristics of the surface material (Azzoni et al. 1995; Agliardi and Crosta 2003; Crosta and Agliardi 2004; Frattini et al. 2012).

The temporal–spatial probability $P(I|T)$ is the probability that the exposed element is affected by the hazard at the time of its occurrence (Fell et al. 2005). It depends on the mobility of the exposed element, and it is usually assessed by assuming an average behaviour of the exposed element (Bunce et al. 1997; Budetta 2004; Michoud et al. 2012), without a discrimination based on season, weather or daylight. For example, for all the vehicles which pass below a single landslide, $P(I|T)$ can be evaluated as the proportion of time in a year a vehicle will be in the path of the landslide (Fell et al. 2005). This approach is suitable for the assessment of expected annual losses but can result in a large underestimation of maximum individual risk for people.

According to the glossary of terms for the risk assessment of the International Society of Soil Mechanics and Geotechnical Engineering (ISSMGE) Technical Committee, physical vulnerability is defined as the degree of loss to a given element or set of elements within the area affected by a hazard (http://140.112.12.21/issmge/tc304.htm). The methods for the estimation of physical vulnerability have been developed and well established for earthquake (e.g. Kappos et al. 2006) and flood risk (e.g. USACE 1996). On the contrary, the quantitative assessment of vulnerability to rockfall is made difficult by the lack of accurate damage data and the inherent complexity of rockfall kinematics and interaction (Agliardi et

al. 2009). Vulnerability in rockfall depends on rockfall intensity (e.g. velocity and volume), the relative location of the vulnerable element in relation to the rockfall trajectory and the characteristics of the exposed elements (construction materials, state of maintenance, age). For site-specific vulnerability assessment, Agliardi et al. (2009) simulated the energy of rockfall impacts against each building damaged from velocity values, by means of a numerical back calibration of the event, and got the empirical vulnerability function of kinetic energy (Mavrouli and Corominas 2010). However, the difficulty in assessing rockfall intensity, the lack of data regarding the characteristics of the exposed elements and their potential damage makes the assessment of vulnerability extremely uncertain (Uzielli et al. 2008).

From the above "Introduction", it is clear that a number of quantities needed for rockfall risk assessment suffer from both epistemic and aleatory uncertainty (Baecher and Christian 2003). Epistemic uncertainty refers to the uncertainty due to the lack of knowledge on a variable. It includes measurement uncertainty, statistical uncertainty (due to limited information) and model uncertainty (Nadim et al. 2005). Epistemic uncertainty can be reduced, for example, by increasing the number of samples or by improving the measurement method and technology (Wang et al. 2012). In rockfall risk analysis, this uncertainty affects the location and volume of the rockfall source, the scale or resolution of the topographic data, the selection for the modelling method and the parameters used for modelling. On the other hand, aleatory uncertainty refers to the natural randomness of a variable. In rockfall risk analysis, aleatory uncertainty affects the topography of the slope and the mechanics property of the rockfall source areas, the latter being dependent on lithology, random distribution of fractures in rock or geological movement experience. Although several authors (e.g. Hoffman and Hammonds 1994; Paté-Cornell 1996; Parry 1996; Merz and Thieken 2005) underline the necessity of keeping the distinction between aleatory and epistemic uncertainty in the analyses, others (Hora 1996; Hofer 2001) observe that sometimes it is difficult to distinguish between the two types of uncertainty, especially when modelling the occurrence or the impacts of extreme physical phenomena, which can be outside our direct experience. In this work, no distinction is made among epistemic and aleatory uncertainties, being strongly connected.

This study is aimed at the following:

- the identification and quantification of the uncertainties and error propagation in risk analysis;
- the development of a new approach for the assessment of the uncertainty connected with restitution and friction coefficients in rockfall run-out modelling;
- the assessment of rockfall risk for people at Feifeng Mountain southern slope, considering different weather conditions.

Methodology

Rockfall risk assessment

In this paper, rockfall risk assessment is based on two risk measures of loss of life (Jonkman et al. 2003). The first is the individual risk (IR), defined, after Bottelberghs (2000), as the probability that an average unprotected person, permanently present at a certain location, is killed due to a rockfall (Fell et al. 2005):

$$\mathrm{IR} = P(L)\cdot P(T|L)\cdot V \tag{1}$$

where $P(L)$ is the annual probability of occurrence of a rockfall event in a given magnitude (i.e. volume) class, $P(T|L)$ is the probability for blocks related to a rockfall event to reach the exposed elements (i.e. reach probability), and V is the vulnerability (i.e. expected degree of loss) of a given exposed element.

The second risk measure is a descriptor of societal risk, i.e. the expected value of the number of fatalities per year, in the literature often referred to as the potential loss of life (PLL):

$$\mathrm{PLL} = P(L)\cdot P(T|L)\cdot P(I|T)\cdot V\cdot n \tag{2}$$

where $P(I|T)$ is the probability that a given exposed element is at the impact location at the time of impact (i.e. temporal–spatial probability or exposure), and n is the number of exposed people with vulnerability V.

For rockfall study, it is extremely complex to define $P(L)$ value. Assuming that rockfall occurrence follows a Poisson distribution (Crovelli 2000; Straub and Schubert 2008; Frattini et al. 2012), the annual probability of occurrence for rare events can be approximated in practice as the annual frequency, being the numerical difference very small (<5 % for annual frequency of <0.1; Hungr and Beckie 1998). Hence, the probability of occurrence can be derived from a magnitude–cumulative frequency (MCF) distribution of rockfall events. As several authors demonstrated (Hungr et al. 1999; Dussauge et al. 2003; Malamud et al. 2004), this distribution can be described by a power law, as:

$$\log N(M > M_o) = N_o + b\cdot \log M \tag{3}$$

where $N(M)$ is the cumulative annual frequency of rockfall events exceeding a given magnitude, M_o; N_o is the total annual number of rockfall events with magnitude larger than 1 m^3, and b is the power law exponent that should be based on complete local rockfall inventory.

The reach probability for a location, $P(T|L)$ is here evaluated as the ratio of the total number of blocks passing a specified location to the total number of blocks launched in the model (Agliardi et al. 2009). When the considered slope is steep and almost planar (i.e. its topography is neither significantly channelled nor convex), the use of 2D rockfall run-out modelling approaches can be considered appropriate for local-scale analysis. However, 3D effects such as lateral dispersion can be observed even on planar slopes due to the effect of slope roughness (Agliardi and Crosta 2003; Frattini et al. 2012). Moreover, 2D models are easier to calibrate where data available for calibration are scarce. In this work, a lumped mass approach is used to calculate energy, velocity and bounce height of falling blocks along 2D slope profiles. Simulation outputs relevant for hazard and risk assessment are the maximum height and velocity along the slope and the distribution of arrested blocks. For 2D simulation, slope profiles have been extracted from a 3D point cloud derived from terrestrial laser scanning, along lines assumed a priori as the most likely rockfall paths. The calibration of normal and tangential coefficients of restitution and the rolling

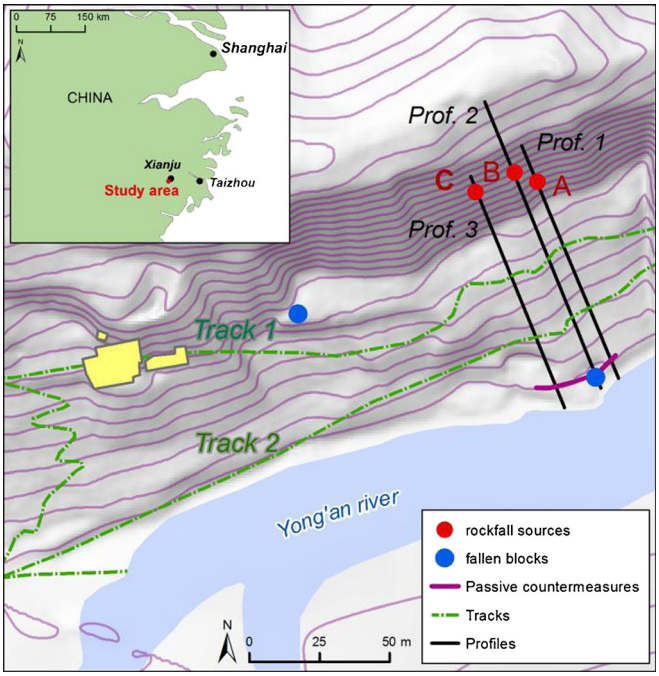

Fig. 1 Study area location and topographic map of the Feifeng Mountain southern slope, with profiles used for simulation and tourist tracks along the study area

friction coefficient was performed by back calibration of historical events. For the temporal–spatial probability, $P(I|T)$, the exposed elements considered in this study are people moving in the area potentially affected by rockfalls. The temporal–spatial probability is then calculated using the following equation (after Fell et al. 2005):

$$P(I|T) = \frac{n}{24} \cdot \frac{L}{1,000} \cdot \frac{1}{v} \quad (4)$$

where n is the number of exposed elements per day moving in the area threatened by rockfalls, characterised by length L (in meters) depending on the considered rockfall scenario, and v is the average velocity (in kilometre per hour) of the moving elements.

In this study, we focus on the physical vulnerability of human beings to rockfall only. Because of the lack of damage statistics and the scarcity of published studies proposing vulnerability curves (Hungr et al. 1999; Corominas et al. 2005; Agliardi et al. 2009), physical vulnerability is difficult to estimate. We assume that, since the velocity of rockfall is usually too high for people to escape, the vulnerability for walking people could be defined as 1 (e.g. all rockfall impacts on people result in death). For people sailing on the boats, a vulnerability of 0.5 was assumed, since in case of impact, only part of the boat would be destroyed.

Uncertainty evaluation

To calculate how the uncertainty propagates along the risk assessment algorithm and affects the final results, a first-order second-moment procedure has been adopted (Baecher and Christian 2003). The method consists in the truncation of Taylor's series expansion, keeping only the first-order terms. It provides an estimate of the mean and the variance (first two moments) of the output through computation of its derivative to the input at a single point (e.g. in Baecher and Christian 2003; Uzielli et al. 2008). The first-order approximation of uncertainty for Eq. 2, aimed at the calculation of PLL, leads to:

$$1 + \Omega^2_{\mathrm{PLL}} = \left(1 + \Omega^2_{P(L)}\right)\left(1 + \Omega^2_{P(T|L)}\right)\left(1 + \Omega^2_{P(I|T)}\right)\left(1 + \Omega^2_{V}\right) \quad (5)$$

where Ω is the coefficient of variation, defined as the ratio between the standard deviation (σ) and the expected value (μ) of the variable.

In this paper, the assignment of Ω values for random variables was performed in different ways. For the coefficients of variation of rockfall run-out parameters (i.e. coefficients of restitution and rolling friction), a specific semi-quantitative methodology was developed. In other cases (e.g. for the number of exposed elements, n, and for their velocity, v), the assignment of Ω values relies on statistical data. Otherwise, for the annual probability of occurrence, vulnerability and the reach probability, Ω values were assigned according to expert knowledge, since the values proposed in the literature for random variables in risk assessment (e.g. Harr 1996; Merz et al. 2004; Kaynia et al. 2008) were adaptable only to the specific case studies. Uncertainty, in fact, is strictly related to the intrinsic characteristics of each phenomenon and to the level of knowledge of the system.

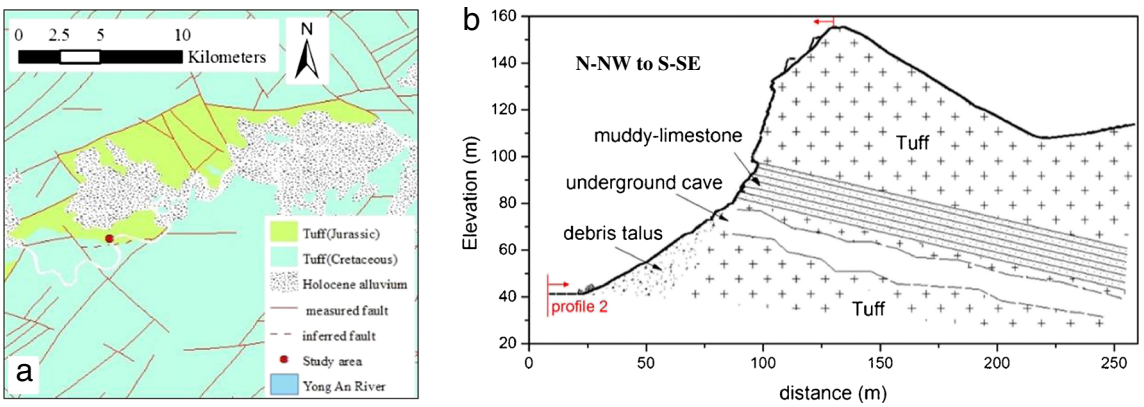

Fig. 2 Study area geology. **a** Regional geological setting, **b** typical lithological profile of the Feifeng Mountain southern slope (profile 2) with position of the underground cave

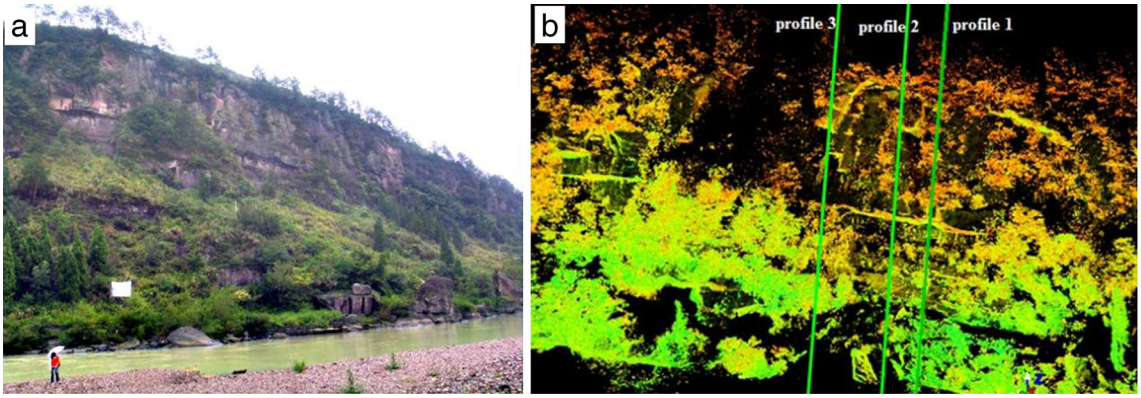

Fig. 3 Feifeng Mountain southern slope. **a** Photo from the south-western side of the study area, **b** 3D points cloud collected through a terrestrial laser scanner

Case study

The large underground mines of Feifeng Mountain, located at Zhejiang Province (E China, Fig. 1), were excavated in tuffaceous rocks to obtain building stones in the ancient China. At the toe of the southern mountain slope, the Yongan River provides a river drifting tourist resort. Because of steep terrain and the occurrence of weak rock masses (i.e. weathered tuffs with thick soft layers) damaged by ancient mining practices, the area is seriously affected by rockfalls threatening human life.

The study area lies at the contact between Upper Jurassic and Upper Cretaceous volcano-sedimentary units (Fig. 2) (RGSTZJ 1978). The Upper Jurassic units are dominant in the area and composed of cinerite tuff, locally with angular gravel and sandstone. The Upper Cretaceous units, composed of amaranth, silicic tuff, locally with sandstone and conglomerate, outcrop nearby the bank of Yongan River. Holocenic alluvium, mainly consisting of loose gravel and sandy clay, also outcrops along the Yongan River. Considering the southern slope of the Feifeng Mountain where the ancient caves are located, we observe the presence of a soft muddy limestone layer separating different tuffaceous units. The thickness of the soft layer is about 15 m and plays an important role in the stability of the slope (Fig. 2). Three main faults control the structural setting of Feifeng Mountain (Fig. 2): a thrust-compressional fault, with dip of 70° to 80° and dip direction of 300°; a NW fault, with dip of 75° to 85°and dip direction of 210°; and a EW fault near Feifeng Mountain.

The detailed geometry of southern slope (Fig. 3) was obtained by using the Leica ScanStation 2 terrestrial laser scanner (TLS). The survey was performed from the toe of the cliff at a distance of about 100 m, with an accuracy of 6 mm at 50 m and a point density between 5 and 10 mm, depending on the distance between the scanner and the surveyed points (Fig. 3). TLS provided a 3D point cloud that was used for 2D modelling profile extraction and rock mass characterization (Fig. 3).

Risk analysis

Identification of rockfall source

The rock mass forming the studied slope was characterised by identifying 57 daylighting discontinuity planes using the TLS point cloud and the software COLTOP 3D (Jaboyedoff et al. 2007). Discontinuities cluster in five main joint sets (Fig. 4) statistically characterised in terms of their mean vector orientations (poles) and dispersion (angular variability limits corresponding to 2 and 3 standard deviations, respectively, according to Priest 1985). Discontinuity persistence ranges between 2 and 15 m, and the aperture is tight to open (from 1 mm to 10 cm).

A kinematic analysis of feasible modes of failure, generated by critical joint sets, allowed to outline the expected rockfall source areas on the cliff and to constrain potential volume scenarios. Basic failure modes are controlled by five main joint sets, allowing for toppling (joint set 4), planar sliding (joint sets 1 and 2), and wedge failure (joint sets 2 and 3).

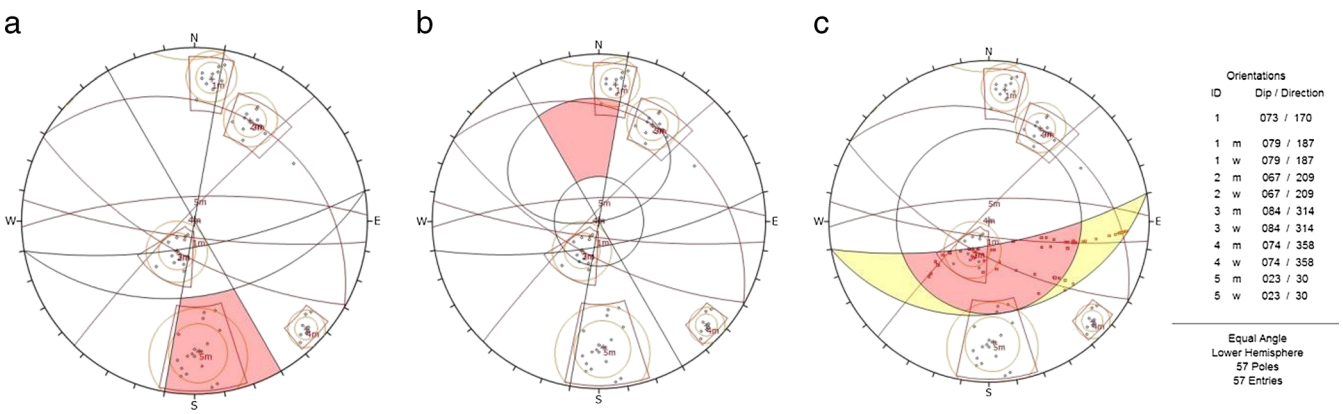

Fig. 4 Kinematic slope stability analysis for main joint sets (the poles in *pink area*): **a** toppling, **b** plane sliding and **c** wedge failure

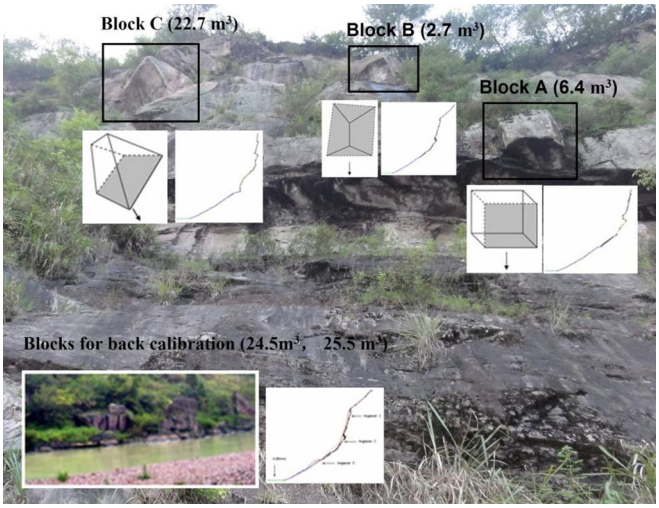

Fig. 5 Main characteristics of unstable blocks A, B and C used for calibration and their profiles shape

Site investigation and ground truth allowed detecting field evidence of block instabilities corresponding to critical failure modes within the source areas identified by geomechanical site characterization. In particular, three blocks (A, B and C) were recognised as most probable rockfall sources (Fig. 5). The stability of block A is controlled by joints 1 and 5. The stability of block B is controlled by joints 2 and 5. The stability of block C is controlled by joints 1, 4 and 5. Moreover, a database of more than 60 blocks corresponding to past rockfall events measured on the surface of the southern slope was prepared.

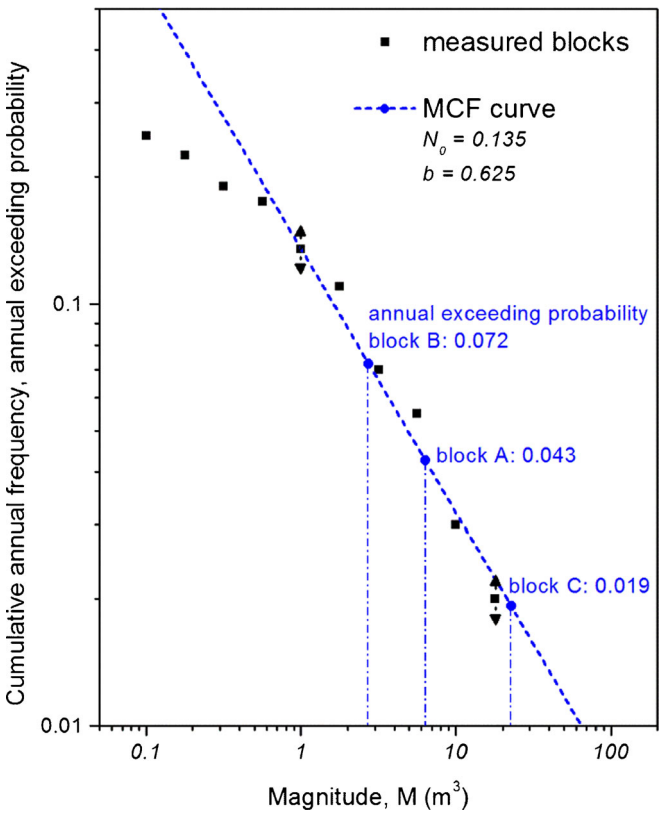

Fig. 6 Magnitude–cumulative frequency curve for rockfall events occurred in the study area ($N=27$) over a 200-year period. Annual exceedance probabilities for the three most unstable blocks are reported

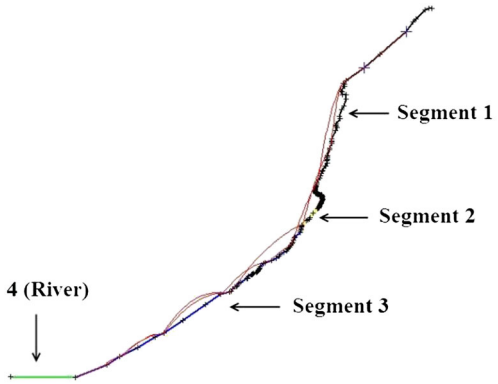

Fig. 7 Slope profile, sectors and rockfall trajectories used for the back calibration of the two historical events

Annual probability of occurrence, $P(L)$

To define $P(L)$ by means of MCF relationships, block volume data collected in the field have been used. Since the historical database for smaller blocks is probably incomplete, only 27 blocks with a volume larger than 1 m³ were used to set up the MCF curve. The resulting curve shows a power-law behaviour at magnitude greater than 1 m³ with a power-law exponent equal to −0.625 (Fig. 6). Based on historical records, excavation of the caves ended up about 200 years ago. This time constraint was assumed as the time interval during which the 27 rockfall events happened. Hence, the parameters N_o and b in Eq. (2) were defined as 0.135 (27/200) and −0.625, respectively. The annual exceedance probability of the three blocks was therefore calculated, on the basis of the MCF curve, as $P(L)_A=0.043$, $P(L)_B=0.072$ and $P(L)_C=0.019$. Considering the large uncertainties in the procedure adopted for defining $P(L)$ (e.g. completeness of the inventory, selection of the time frame for frequency calculation, MCF parameterization), large uncertainty values, Ω, were assigned to $P(L)$, corresponding to 0.2, 0.3 and 0.2 for blocks A, B and C, respectively. The Ω value for block B is assumed to be higher because of the smaller size of the block, which makes larger the uncertainty related to the adoption of MCF relationship.

The reach probability, $P(T|L)$

The run-out distance, bounce height and velocity of the three blocks (A, B and C) were simulated along the 2D slope profiles

Table 1 Mean values for slope parameters resulting from back calibration of past events

Slope segments	Normal restitution coefficient	Tangential restitution coefficient	Rolling friction angle
1 (tuff)	0.45	0.85	30
2 (limestone)	0.43	0.81	32
3 (talus)	0.31	0.71	38
4 (river)	0	0	90

Table 2 Diversity scores assigned to the slope profiles associated to each potentially unstable blocks A, B and C (Fig. 5). The diversity scores are as follows: 1=very similar, 2=similar, 3=slightly different, 4=different and 5=very different

Factors	Block A Diversity scores	Block B	Block C
Slope material	1	1	2
Slope shape	2	1	4
Block shape	3	1	1
Block location	3	2	2
Block size	3	4	1

by Rocfall™ (Rocscience, Inc. 2002). This simulation model is based on a kinematic (lumped mass) approach for trajectories calculation (Stevens 1998). The energy dissipation by bouncing and rolling is simulated by using empirical restitution coefficients and rolling friction angle (Stevens 1998). The model provides as output values of velocity and bounce height for any point along a predictive slope profile and the locations of arrested blocks. Among the parameters used in the model, the slope profile geometry and the coefficients of restitution and friction are the most significant. The former was acquired on the field by using a TLS. The other parameters were obtained by back calibrating two historical rockfall events. For this reason, the slope was initially divided into four sectors based on superficial lithology and material: tuff, muddy limestone, debris talus and river. Then, the coefficients of restitution and friction have been assigned to each sector by back calibration of the historical events (Fig. 7, Table 1). The same parameter values have been assigned to slope profiles of rockfall scenarios A, B and C.

To account for the uncertainty related to restitution and friction coefficients, the simulation was performed with a stochastic approach that allows, at each impact, to randomly sample, the value of the parameter from a normal distribution with given mean and standard deviation. The standard deviations of coefficients of restitution and friction are normally defined by an expert knowledge (Wang et al. 2012). Given the importance in the selection of appropriate and non-arbitrary values of standard deviations, a semi-quantitative methodology was developed.

This methodology is based on the degree of difference between the topographic and physical characteristics of a given slope profile to be used for 2D rockfall prediction and those of a reference profile used for parameter calibration; higher diversity is likely to correspond to higher uncertainty about rockfall run-out parameters. The diversity is assessed for a few factors controlling the rockfall dynamics: slope shape, slope materials, source of area position along the slope, shape and size of the blocks (Table 2).

The methodology involves four steps of evaluation:

1. for each *i*th slope profile to be used for predictive modelling, comparison with the reference slope profile and assignment of the diversity score for each controlling factor is accomplished;
2. weighting of the controlling factors by means of the analytic hierarchy process (AHP);
3. calculation of a weighted sum of all the controlling factors to assess the index of diversity for each slope profile, D_i;
4. transformation of D_i into Ω values.

For each model profile, the similarity between these factors and those characterising the reference profile has been expressed by assigning a diversity score ranging from 1 to 5 (Table 2).

As an example, block A presents a slope profile with the same material as the reference profile (slope material diversity score of 1) and a similar shape (slope shape score of 2). The characteristics of the block are slightly different (block shape score, 3; block location, 3; and block size, 3) as illustrated in Fig. 5.

Controlling factors are then weighted by using the AHP (Saaty 1980; Saaty and Vargas 2001; Nefeslioglu et al. 2013). Numerical scores are assigned by means of subjective judgement on the relative importance of each factor, by the construction of an AHP pairwise comparison matrix. In this matrix, each factor is rated against the others by assigning a relative dominant score between 1 (equal dominance) and 9 (strongly dominant) (Table 3). The maximum eigenvalue (λ_{max}) of the AHP pairwise comparison matrix and its corresponding eigenvector provide the weights of the factors. To quantify the consistency and reliability of AHP pairwise comparison matrix, the consistency ratio (CR) was calculated. A CR lower than 0.1 is normally acceptable (Ayalew et al. 2004), although this depends on the objective of the study (Wang et al. 2013). In this study, a CR of 0.03 was obtained.

The diversity index of potentially unstable block *i* (*i*=A, B, and C) is calculated as the weighted sum of the diversity scores:

$$D_i = \sum_j d_{i,j} \cdot w_j \qquad (6)$$

where $d_{i,\,j}$ is the diversity score of the unstable block *i* for the controlling factor *j*, and w_j is the weight of controlling factor *j*. For example, the calculation of D_A leads to $D_A=(1\times0.46)+(2\times0.24)+(3\times0.08)+(3\times0.05)+(3\times0.17)=1.8$

Table 3 AHP pairwise comparison matrix for calculating weights. The rating of comparison is the following: 1=equal, 3=moderately higher, 5=higher, 7=strongly higher and 9=extremely higher. Values 2, 4, 6 and 8 are intermediate values. Consistency ratio is equal to 0.03

	Slope material	Slope shape	Block shape	Block location	Block size	Weight
Slope material	1	3	5	7	3	0.46
Slope shape	1/3	1	4	5	2	0.24
Block shape	1/5	1/4	1	2	1/3	0.08
Block location	1/7	1/5	1/2	1	1/5	0.05
Block size	1/3	1/2	3	5	1	0.17

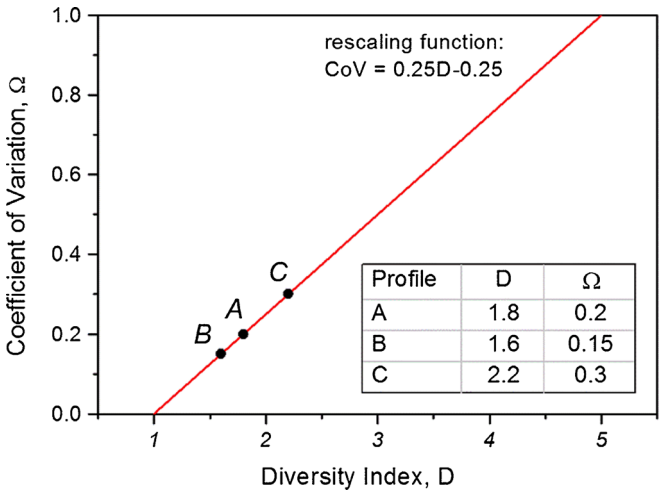

Fig. 8 Linear relationship between Ω and D values

To assess Ω, a linear relationship between D and Ω is proposed, allowing to rescale the values of index D in Ω values ranging from 0 to 1 (Fig. 8). Finally, from the Ω value, the standard deviation of restitution and rolling friction coefficients are obtained (Table 4).

The simulation of rockfall propagation was performed for each unstable block using the model parameters presented in Table 5.

The distribution of the arrested blocks was used to assess the reach probability as the percentage of blocks that stop uphill to a certain location along the slope. Based on the results of the models (Figs. 9 and 10), the reach probabilities of block A in correspondence to track 1, track 2 and the river bank (Fig. 3) are 0.96, 0.095 and 0, respectively; for block B, 0.998, 0.58 and 0, respectively; and for block C, 0.977, 0.551 and 0.056, respectively.

The uncertainty associated to reach probability is explicitly considered within the stochastic simulation of rockfall run-out. For this reason, only a small residual uncertainty (Ω=0.1) is associated to the reach probability, $P(T|L)$, of the three potentially unstable blocks.

Temporal–spatial probability, $P(I|T)$

In the study area, two groups of exposed elements are considered significant: (1) the tourists visiting the underground caves in Feifeng Mountain, moving along the two existing tracks (Fig. 1), and (2) the tourists drifting in the Yongan River (Figs. 1 and 3), which are, by far, the most numerous. The record of visitors to the area was provided by the administrative department for river navigation tourism and shows that the temporal–spatial probability for the tourists is strongly affected by weather conditions. This is especially true for the second group, because the number of tourists drifting in the Yongan River increases greatly during dry days and dramatically decreases during rainy days. From local rainfall records, it can be observed that the months with heavy rainfall are June, July and August, for a total of about 90 days. Considering the characteristics of groups 1 and 2, it was possible to calculate the temporal–spatial probability (Table 6) based on Eq. (4). In this formulation, the large uncertainties derive from the number of exposed elements, n, and the transit velocity of the elements at risk, v. The uncertainty is strictly related to the characteristics of each site-specific phenomenon and the quality of the available data. The assignment of Ω values was performed based on the statistic information given by the local administrative department for river navigation tourism and a statistic analysis on velocity of boats drifting in the river (Table 7).

Table 5 Model parameters used in the simulation of rockfall propagation

Parameters	Value
Block volume	Fig. 2
Number of simulated blocks	1,000
Coefficient of normal restitution	Table 4
Coefficient of tangential restitution	Table 4
Rotational friction angle	Table 4
Initial velocity (m/s)	0
Surface roughness (°)	2
Minimum velocity cut-off (m/s)	0.1

Vulnerability, V

Evaluating the expected damage to each exposed element is a difficult and uncertain operation. Due to the large volume and expected velocity of potential blocks (Fig. 9), the vulnerability of the tourists is assumed as 1; in case of impact, the person would die. As shown in Figs. 9 and 10, only block C has the possibility to reach the river, where the exposed elements are the tourists on the drifting boats. For risk calculation, eight tourists for each boat were considered on average, and a vulnerability of 0.5 was assumed; in case of impact, only part of the boat would be destroyed, thus allowing half of the people to survive. Giving the large uncertainty associated to this vulnerability value, we assigned a coefficient of variation (Ω) equals to 0.5.

Rockfall risk to people

By adopting Eqs. (1), (2) and (5), the IR and the PLL and related uncertainties have been calculated for each rockfall scenario at

Table 4 Statistical parameters (mean, μ; standard deviation, σ) of normal distribution of coefficients used in the simulation for blocks A, B and C

Sector	Normal restitution coefficient				Tangential restitution coefficient				Rolling friction angle			
	μ	σ_A	σ_B	σ_C	μ	σ_A	σ_B	σ_C	μ (°)	σ_A	σ_B	σ_C
1 (tuff)	0.45	0.09	0.07	0.14	0.85	0.17	0.13	0.26	30	6	4.5	9
2 (siltstone)	0.43	0.09	0.06	0.13	0.81	0.16	0.12	0.24	32	6.4	4.8	9.6
3 (talus)	0.31	0.06	0.05	0.09	0.71	0.14	0.11	0.21	38	7.6	5.7	1.8
4 (river)	0		0		0		0		90		0	

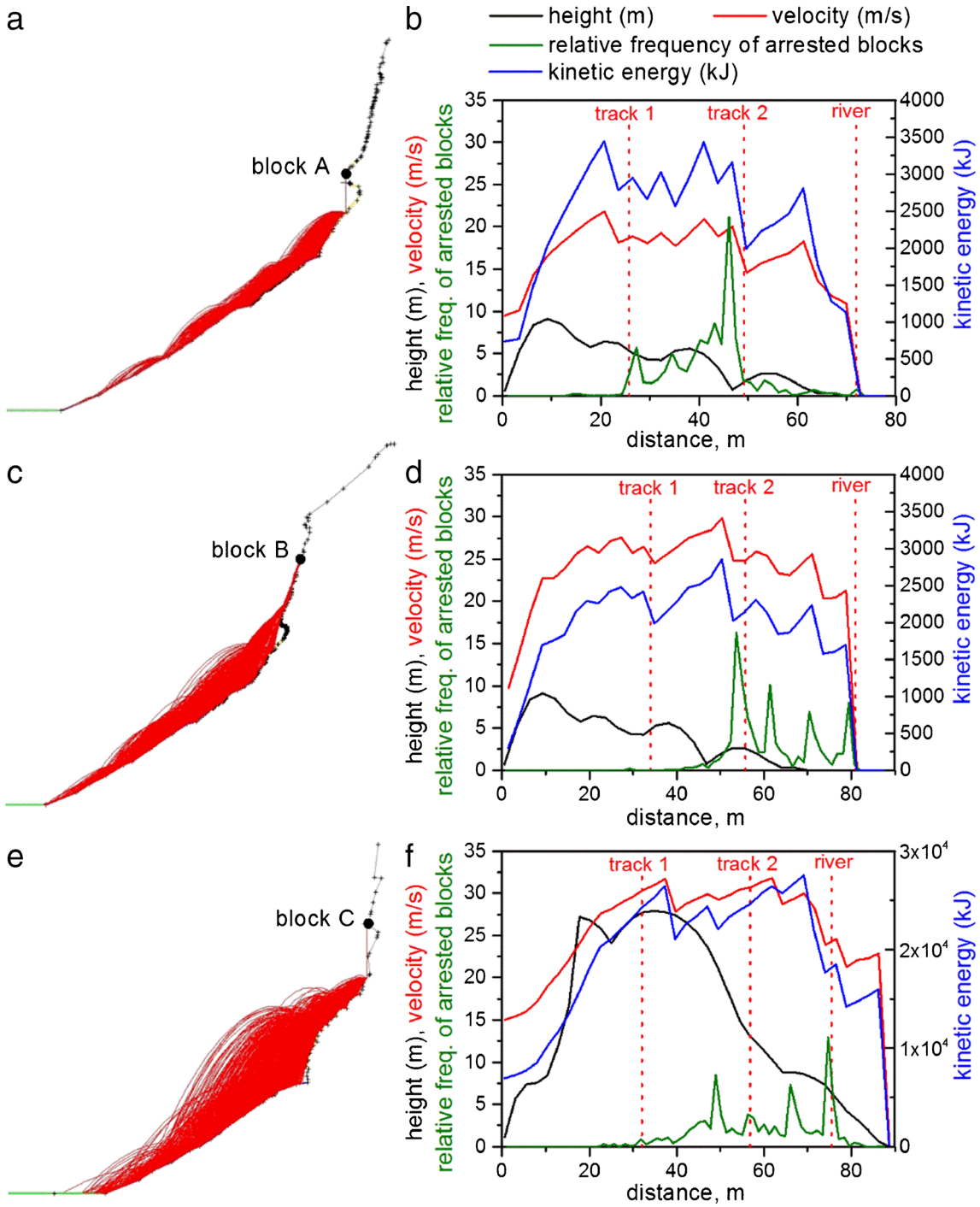

Fig. 9 Rockfall simulation for potentially unstable blocks. **a**, **c**, **e** Rockfall trajectories. **b**, **d**, **f** Plots representing the percentage of arrested blocks, bounce height, translational velocity and total kinetic energy as a function of the distance from the source area along the slope

three different locations along the slope (track 1, track 2 and river) (Fig. 1, Table 7).

Risk evaluation

The values of IR (Table 7) are significantly above the limit defined by the tolerability line (10^{-5} per year for new developments, 10^{-4} per year for existing developments) for non-volunteer risk such as rockfalls, as proposed by Geotechnical Engineering (1998). This means that in the study area, the individual risk is not acceptable, and some actions are requested in order to lower the risk. It must be considered that a passive countermeasure is already present at the toe of the slope (Table 2), and it was not taken into account for risk assessment.

Regarding the societal risk, the following scenarios have been analysed: one person was killed by blocks A, B and C at tracks 1 and 2 during dry or rainy days, and eight people were killed by

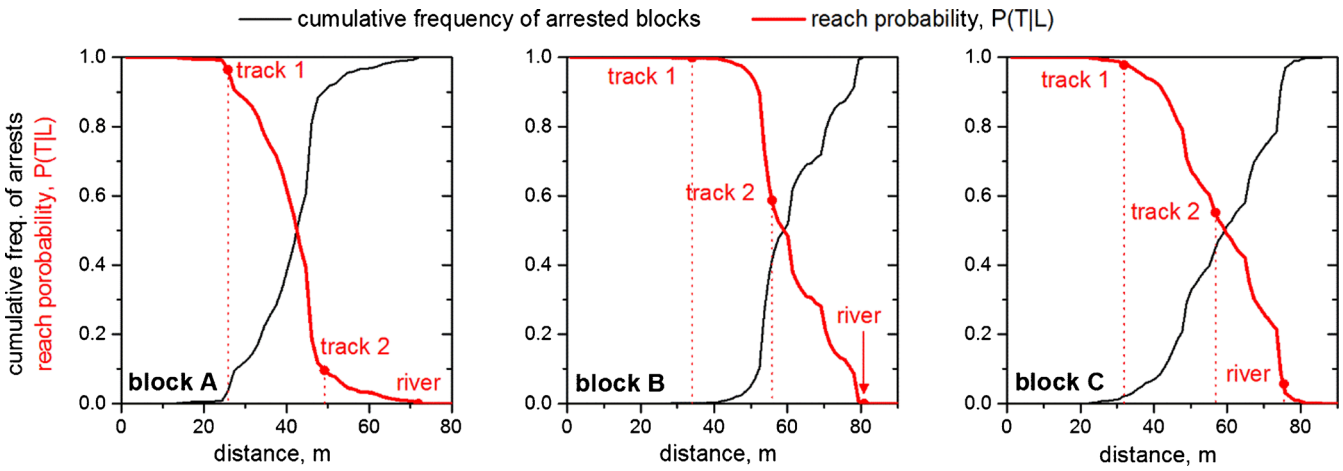

Fig. 10 Cumulative frequency of the arrested blocks and reach probability as a function of the distance from the source area for the potentially unstable blocks A, B and C

block C along the river during dry or rainy days. In order to plot the societal risk as F–N curve, the annual exceedance probability of each scenario and the number of deaths were extracted from PLL and used as coordinates in the F–N chart. Then, the F–N curve was built up by summing the different scenarios (Fig. 11). The F–N curve for societal risk falls within the as low as reasonably practicable (ALARP, Smith 1990; HSE 1992) between the objective and the limit thresholds for acceptability defined for Hong Kong by Geotechnical Engineering (1998) (Fig. 11). Considering the uncertainty (Table 7), the societal risk could be higher or lower than the mean value shown in Table 7, but still within the ALARP zone.

Discussion and conclusion

The overall societal risk calculated summing up the different scenarios (Fig. 11), also considering the related uncertainties, lies within the ALARP zone and therefore requires some mitigation actions to be taken in order to reduce the risk level. These could include the following:

1. Engineering countermeasures to reduce the frequency of rockfall. For instance, the possible unstable blocks could be investigated and removed in advance. Alternatively, since the instability of the three most critical blocks is controlled by apparent joints, rock bolting can be used to stabilise them.
2. Actions to reduce the rockfall run-out. In the study area, the most effective remedial measures may be a retaining wall or an elastoplastic barrier to protect the river bank. Considering the water level fluctuations, the optimal position for these works could be 3 m away from the river bank (Fig. 3). The dimensioning of the retaining wall/barrier could be done based on the behaviour of block C, considering a lateral dispersion of rockfall trajectories, which will determine the length of the

Table 6 Parameters for the calculation of temporal–spatial probability for 14 potential risk scenarios; n = number of people along track 1 or 2, number of boats along the river; L = estimated length of the endangered sector along tracks and river; v = velocity of the people along track 1 or 2, velocity of the boat along the river

Scenario	Weather condition	Block	Track	n	L (m)	v (m/s)	$P(I\|T)$
s1	Dry	A	1	5	7	1	1.5×10^{-3}
s2	Dry	B	1	5	11	1	2.3×10^{-3}
s3	Dry	C	1	5	15	1	3.1×10^{-3}
s4	Rainy	A	1	1	7	1	2.9×10^{-4}
s5	Rainy	B	1	1	11	1	4.6×10^{-4}
s6	Rainy	C	1	1	15	1	6.3×10^{-4}
s7	Dry	A	2	1	7	1	2.9×10^{-4}
s8	Dry	B	2	1	11	1	4.6×10^{-4}
s9	Dry	C	2	1	15	1	6.3×10^{-4}
s10	Rainy	A	2	0	7	1	0
s11	Rainy	B	2	0	11	1	0
s12	Rainy	C	2	0	15	1	0
s13	Dry	C	River	40	15	3	8.3×10^{-3}
s14	Rainy	C	River	5	15	3	1.0×10^{-3}

Table 7 Rockfall risk calculation. $P(L)$, annual exceedance probability of rockfall occurrence; $P(T|L)$, reach probability; $P(I|T)$, temporal–spatial probability; IR, individual risk in terms of annual exceedance probability; PLL, potential loss of life in terms of annual expected number of deaths; Ω, coefficient of variation

Scenario	$P(L)$	$P(T\|L)$	$P(I\|T)$	V	IR	PLL	$\Omega_{P(L)}$	$\Omega_{P(T\|L)}$	$\Omega_{P(I\|T)}$	Ω_V	Ω_{IR}	Ω_{PLL}
s1	0.043	0.964	1.5×10^{-3}	1	4.1×10^{-2}	6.0×10^{-5}	0.2	0.1	0.41	0	0.22	0.48
s2	0.072	0.998	2.3×10^{-3}	1	7.2×10^{-2}	1.6×10^{-4}	0.3	0.1	0.41	0	0.32	0.53
s3	0.019	0.977	3.1×10^{-3}	1	1.9×10^{-2}	5.8×10^{-5}	0.3	0.1	0.41	0	0.32	0.53
s4	0.043	0.964	2.9×10^{-4}	1	4.1×10^{-2}	1.2×10^{-5}	0.2	0.1	1.0	0	0.22	1.05
s5	0.072	0.998	4.6×10^{-4}	1	7.2×10^{-2}	3.3×10^{-5}	0.3	0.1	1.0	0	0.32	1.10
s6	0.019	0.977	6.3×10^{-4}	1	1.9×10^{-2}	1.2×10^{-5}	0.3	0.1	1.0	0	0.32	1.10
s7	0.043	0.095	2.9×10^{-4}	1	4.1×10^{-3}	1.2×10^{-6}	0.2	0.1	1.0	0	0.22	1.05
s8	0.072	0.586	4.6×10^{-4}	1	4.2×10^{-2}	1.9×10^{-5}	0.3	0.1	1.0	0	0.32	1.10
s9	0.019	0.551	6.3×10^{-4}	1	1.0×10^{-2}	6.5×10^{-6}	0.3	0.1	1.0	0	0.32	1.10
s10	0.043	0.095	0	1	4.1×10^{-3}	0	0.2	0.1	0.51	0	0.22	0.57
s11	0.072	0.586	0	1	4.2×10^{-2}	0	0.3	0.1	0.51	0	0.32	0.62
s12	0.019	0.551	0	1	1.0×10^{-2}	0	0.3	0.1	0.51	0	0.32	0.62
s13	0.019	0.056	8.3×10^{-3}	0.5	5.3×10^{-4}	3.5×10^{-5}	0.3	0.1	0.2	0.5	0.61	0.66
s14	0.019	0.056	1.0×10^{-3}	0.5	5.3×10^{-4}	4.43×10^{-6}	0.3	0.1	1	0.5	0.61	1.32

V vulnerability

countermeasures. Lateral dispersion can be assumed from literature values (e.g. 20° according to empirical observations, Bozzolo and Pamini 1986; Evans and Hungr 1993; Azzoni et al. 1995) or explicitly modelled by using 3D simulation models (Volkwein et al. 2011; Frattini et al. 2012). Besides retaining wall/barrier, forest management can be used to reduce the rockfall run-out. On site survey revealed that at least 12 fallen blocks were stopped by trees along the slope. The plantation of new stronger trees on the southern slopes of Feifeng Mountain could efficiently protect the Yongan River.

3. Actions to reduce the probability of tourists being below a rockfall when it occurs. Since the two tracks on the southern slope are not strictly needed for visiting the underground caves, it is suggested to close them.

The uncertainty about the estimated rockfall risk, expressed as 1 standard deviation, ranges between 48 and 132 % of the mean value. Hence, the error rate can be extremely high, depending on the large uncertainties in the estimation of the onset probability and the temporal–spatial probability. These results demonstrate the importance of accounting for uncertainty in rockfall risk modelling. For scientists, this provides a tool to identify potential needs for the improvement in data collection, in order to decrease the uncertainty. For instance, from our analysis the assessment of

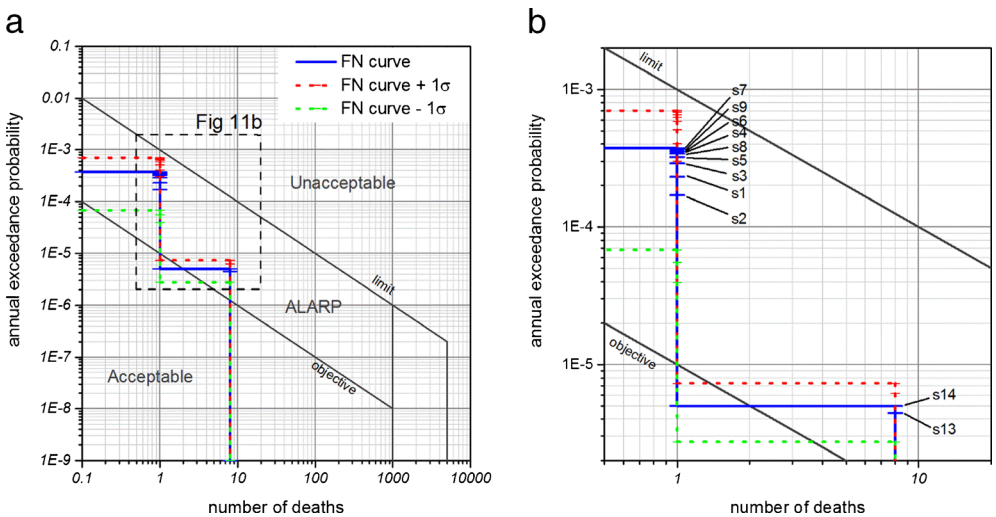

Fig. 11 F–N curves for rockfall societal risk considering all scenarios. Scenarios s10, s11 and s12 are not in the plot, because the number of people at risk is equal to 0 (see Tables 6 and 7)

the temporal–spatial probability is the most critical and uncertain step of the risk analysis procedure. Hence, a better monitoring of the movement of people at risk needs to be implemented. For administrators and decision makers, accounting for the uncertainty could be extremely important to have an evaluation of the degree of confidence of the results to be used for the implementation of mitigation actions.

Acknowledgments

The authors would like to thank the support of China Postdoctoral Science Foundation (no. 2013M530722), the Chinese Academy of Sciences Knowledge Innovation Project important direction project (KZCX2-YW-Q03-02), the National Natural Science Foundation of China (40502027), the Chinese Academy of Sciences Key Deployment Project (KZZD-EW-05-02) and the Italian PRIN Project "Previsione spazio-temporale di fenomeni franosi ad alto impatto nel quadro dei cambiamenti del regime delle piogge" (2010E89BPY_007). The authors wish to express their appreciation to two anonymous reviewers, whose detailed comments were very helpful in improving the manuscript.

References

Agliardi F, Crosta GB (2003) High resolution three-dimensional numerical modelling of rockfalls. International Journal of Rock Mechanics and Mining Sciences 40(4):455–471

Agliardi F, Crosta GB, Frattini P (2009) Integrating rockfall risk assessment and countermeasure design by 3D modelling techniques. Natural Hazards and Earth System Sciences 9(4):1059–1073

Ayalew L, Yamagishi H, Ugawa N (2004) Landslide susceptibility mapping using GIS-based weighted linear combination, the case in Tsugawa area of Agano River, Niigata Prefecture, Japan. Landslides 1(1):73–81

Azzoni A, La Barbera G, Zaninetti A (1995) Analysis and prediction of rockfalls using a mathematical model. International Journal of Rock Mechanics and Mining Sciences & Geomechanics Abstracts 32(7):709–724

Baecher GB, Christian JT (2003) Reliability and statistics in geotechnical engineering. Wiley, London, p 605

Bottelberghs PH (2000) Risk analysis and safety policy developments in the Netherlands. J Hazard Mater 71:59–84

Bozzolo D, Pamini R (1986) Simulation of rock falls down a valley side. Acta Mechanica 63:113–130

Budetta P (2004) Assessment of rockfall risk along roads. Nat Hazards Earth Syst Sci 4:71–81

Bunce CM, Cruden DM, Morgenstern NR (1997) Assessment of the hazard from rock fall on a highway. Can Geotech J 34:344–356

Cascini L, Bonnard C, Corominas J, Jibson R, Montero-Olarte J (2005) Landslide hazard and risk zoning for urban planning and development. State of the art report (SOA7). In: Hungr O, Fell R, Couture R, Eberthardt E (eds) Proceedings of the international conference on "landslide risk management", Vancouver (Canada). Taylor and Francis, London, pp 199–235

Copons R, Vilaplana J, Linares R (2009) Rockfall travel distance analysis by using empirical models (SolAd'Andorra la Vella, Central Pyrenees). Natural Hazards and Earth System Sciences 9(6):2107–2118

Corominas J (1996) The angle of reach as a mobility index for small and large landslides. Canadian Geotechnical Journal 33:260–271

Corominas J, Copons R, Moya J, Vilaplana JM, Altimir J, Amigò J (2005) Quantitative assessment of the residual risk in a rockfall protected area. Landslides 2:343–357

Crosta GB, Agliardi F (2004) Parametric evaluation of 3D dispersion of rockfall trajectories. Natural Hazards and Earth System Sciences 4(4):583–598

Crosta GB, Agliardi F, Frattini P, Imposimato S (2004) A three-dimensional hybrid numerical model for rockfall simulation. Geophysical Research Abstracts 6:04502

Crovelli RA (2000) Analytic resource assessment method for continuous (unconventional) oil and gas accumulations—the "ACCESS" method: U.S. Geological Survey Open-File Report 00–044, p 34

Dorren LKA, Berger F, Putters US (2006) Real-size experiments and 3-D simulation of rockfall on forested and non-forested slopes. Natural Hazards and Earth System Sciences 6:145–153

Dussauge C, Grasso JR, Helmstetter A (2003) Statistical analysis of rockfall volume distributions: implications for rockfall dynamics. J Geophys Res 108(B6):2286. doi:10.1029/2001JB000650

Evans SG, Hungr O (1993) The assessment of rockfall hazard at the base of talus slopes. Canadian Geotechnical Journal 30(4):620–636

Fell R, Ho KKS, Lacasse S, Leroi E (2005) A framework for landslide risk assessment and management. In: Hungr O, Fell R, Couture R, Eberhardt E (eds) Landslide risk management. Taylor and Francis, London, pp 3–26

Fell R, Corominas J, Bonnard C, Cascini L, Leroi E, Savage WZ (2008) Guidelines for landslide susceptibility, hazard and risk zoning for land use planning. Eng Geol 102:85–98

Frattini P, Crosta GB, Carrara A, Agliardi F (2008) Assessment of rockfall susceptibility by integrating statistical and physically-based approaches. Geomorphology 94(3–4):419–437

Frattini P, Crosta GB, Agliardi F (2012) Rockfall characterization and modeling. In: Clague JJ, Stead D (eds) Landslides types, mechanisms and modeling. Cambridge University Press, Cambridge, pp 267–281, ISBN: 978-1-107-00206-7

Geotechnical Engineering Office (1998) Landslides and boulder falls from natural terrain: interim risk guidelines. GEO Report No. 75. Geotechnical Engineering Office, The Government of the Hong Kong Special Administrative Region

Glade T (2003) Vulnerability assessment in landslide risk analysis. Die Erde 134:121–138

Guzzetti F, Crosta GB, Detti R, Agliardi F (2002a) STONE: a computer program for the three-dimensional simulation of rock-falls. Computers & Geosciences 28(9):1079–1093

Guzzetti F, Malamud BD, Turcotte DL, Reichenbach P (2002b) Power-law correlations of landslide areas in central Italy, Earth Planet. Sci Lett 195:169–183

Harr ME (1996) Reliability-based design in civil engineering. Dover Publication, Inc., Mineola

Hofer BK (2001) Personal epistemology research: implications for learning and instruction. Educ Psychol Rev 13(4):353–382

Hoffman FO, Hammonds JS (1994) Propagation of uncertainty in risk assessments: the need to distinguish between uncertainty due to lack of knowledge and uncertainty due to variability. Risk Analysis 14:707–712

Hora SC (1996) Aleatory and epistemic uncertainty in probability elicitation with an example from hazardous waste management. Reliability Engineering and System Safety 54:217–223

HSE (1992) The tolerability of risk from nuclear power stations. Health and Safety Executive, London

Hungr O, Beckie RD (1998) Assessment of the hazard from rock fall on a highway: discussion. Canadian Geotechnical Journal 35:409

Hungr O, Evans SG, Hazzard J (1999) Magnitude and frequency of rockfalls and rock slides along the main transportation corridors of south-western British Columbia. Can Geotech J 36:224–238

Jaboyedoff M, Metzger R, Oppikofer T, Couture R, Derron M-H, Locat J, Turmel D (2007) New insight techniques to analyze rock-slope relief using Dem and 3D-imaging cloud points: COLTOP-3D. In: Eberhardt E, Stead D, Morrison T (eds) Rock mechanics: meeting Society's challenges and demands. 1st Canada–US rock mechanics symposium. Taylor and Francis, Vancouver

Jones CL, Higgins JD, Andrew RD (2000) Colorado rockfall simulation program version 4.0. Colorado Department of Transportation, Colorado Geological Survey, Colorado

Jonkman SN, Van Gelder PHAJM, Vrijling JK (2003) An overview of quantitative risk measures for loss of life and economic damage. Journal of Hazardous Materials A99:1–30

Kappos AJ, Panagopoulos G, Panagiotopoulos C, Penelis G (2006) A hybrid method for the vulnerability assessment of R/C and URM buildings. B Earthq Eng 4:391–413

Kaynia AM, Papathoma-Köhle M, Neuhäuser B, Ratzinger K, Wenzel H, Medina-Cetina Z (2008) Probabilistic assessment of vulnerability to landslide: application to the village of Lichtenstein, Baden-Württemberg, Germany. Eng Geol 101(1–2):33–48

Malamud BD, Turcotte DL, Guzzetti F, Reichenbach P (2004) Landslide inventories and their statistical properties. Earth Surf Proc Land 29:687–711

Mavrouli O, Corominas J (2010) Vulnerability of simple reinforced concrete buildings to damage by rockfalls. Landslides 7(2):169–180

Merz B, Thieken A (2005) Separating natural and epistemic uncertainty in flood frequency analysis. J Hydrol 309(1–4):114–132

Merz B, Kreibich H, Thieken AH, Schmidtke R (2004) Estimation uncertainty of direct monetary flood damage to buildings. Natural Hazards and Earth System Sciences 4:153–163

Michoud C, Derron M-H, Horton P, Jaboyedoff M, Baillifard F-J, Loye A, Nicolet P, Pedrazzini A, Queyrel A (2012) Rockfall hazard and risk assessments along roads at a regional scale: example in Swiss Alps. Natural Hazards and Earth System Science 12(3):615–629

Nadim F, Einstein H, Roberds W (2005) Probabilistic stability analysis for individual slopes in soil and rock. In: Hungr O, Fell R, Couture R, Eberhardt E (eds) Landslide risk management. Taylor and Francis, London, pp 3–26

Nefeslioglu HA, Sezer EA, Gokceoglu C, Ayas Z (2013) A modified analytical hierarchy process (M-AHP) approach for decision support systems in natural hazard assessments. Computers & Geosciences 59:1–8

Parry GW (1996) The characterization of uncertainty in probabilistic risk assessments of complex systems. Reliability Engineering and System Safety 54:119–126

Paté-Cornell ME (1996) Uncertainties in risk analysis: six levels of treatment. Reliability Engineering and System Safety 54(2–3):95–111

Priest SD (1985) Hemispherical projection methods in rock mechanics. George Allen and Unwin, London, 124p

RGSTZJ (Regional Geology Survey Team of Zhejiang province) (1978) Report of regional geology survey (Xianju County Breadth)

Rocscience, Inc. (2002) ROCFALL-computer program for risk analysis of falling rocks on steep slopes. Version 4.0. Rocscience, Inc, Toronto

Saaty TL (1980) The analytical hierarchy process. McGraw-Hill, New York

Saaty TL, Vargas LG (2001) Models, methods, concepts, and applications of the analytic hierarchy process. Kluwer, Boston, p 333

Smith K (1990) The application of the ALARP principle to safety assessment by the nuclear installations inspectorate. In: Institution of Nuclear Engineers on the use of ALARA in the nuclear industry. Royal Aeronautical Society, London

Stevens W (1998) Rockfall: a tool for probabilistic analysis, design of remedial measures and prediction of rockfalls. M.A.Sc. Thesis, Department of Civil Engineering, University of Toronto, Ontario

Straub D, Schubert M (2008) Modelling and managing uncertainties in rock-fall hazards. Georisk 2:1–15

USACE (U.S. Army Corps of Engineers) (1996) Risk-based analysis for flood damage reduction studies. Engineering Manual 1110-2-1619, Washington, D.C.

Uzielli M, Nadim F, Lacasse S, Kaynia AM (2008) A conceptual framework for quantitative estimation of physical vulnerability to landslides. Eng Geol 102:251–253

Volkwein A, Schellenberg K, Labiouse V, Agliardi F, Berger F, Bourrier F, Dorren LKA, Gerber W, Jaboyedoff M (2011) Rockfall characterization and structural protection—a review. Natural Hazards and Earth System Sciences 11:2617–2651

Wang XL, Zhang LQ, Wang SJ, Agliarid F, Frattini P, Crosta GB, Yang ZF (2012) Field investigation and rockfall hazard zonation at the Shjing Mountains Sutra caves cultural heritage (China). Environmental Earth Sciences 66:1897–1908

Wang XL, Zhang LQ, Wang SJ, Lari S (2013) Regional landslide susceptibility zoning with considering the aggregation of landslide points and the weights of factors. Landslides. doi:10.1007/s10346-013-0392-6

Zhang LQ, Yang ZF, Liao QL, Chen J (2004) An application of the rock engineering system (RES) methodology to rockfall hazard assessment on the Chengdu-Lhasa Highway, China. International Journal of Rock Mechanics and Mining Sciences 41(3):526–527

X. Wang (✉) · L. Zhang · Z. Yang
Key Laboratory of Engineering Geomechanics, Institute of Geology and Geophysics,
Chinese Academy of Sciences,
Beijing 100029, China
e-mail: wxljlu@163.com

P. Frattini · G. B. Crosta · F. Agliardi · S. Lari
Department of Earth and Environmental Sciences,
University of Milano-Bicocca,
Milan 20126, Italy